Supporting Information

Synthesis, stereochemical separation, and biological evaluation of selective inhibitors of human MAO-B: 1-(4-arylthiazol-2-yl)-2-(3-methylcyclohexylidene)hydrazines

Franco Chimenti,[†] Daniela Secci,[†] Adriana Bolasco,[†] Paola Chimenti,[†] Arianna Granese,[†] Simone Carradori,[†] Matilde Yáñez,[§] Francisco Orallo,[§] M. Luisa Sanna,[¥] Bruno Gallinella,[¥] and Roberto Cirilli.[¥]*

Contents

Pharmacological studies

Drugs and chemicals

The drugs, vehicle and chemicals used in the experiments were the new compounds, moclobemide (a generous gift from F. Hoffmann-La Roche Ltd., Basel, Switzerland), dimethyl sulfoxide (DMSO), *R*-(-)-deprenyl hydrochloride, iproniazid phosphate, isatin (purchased from Sigma-Aldrich, Spain), resorufin sodium salt, clorgyline hydrochloride, *p*-tyramine hydrochloride, sodium phosphate and horseradish peroxidase (supplied in the Amplex Red MAO assay kit from Molecular Probes).

Appropriate dilutions of the above drugs were prepared every day immediately before use in deionized water from the following concentrated stock solutions kept at –20 °C: the new compounds and isatin (0.1 mM) in DMSO; *R*-(-)-deprenyl, moclobemide, iproniazid, resorufin, clorgyline, *p*-tyramine and horseradish peroxidase (0.1 M) in deionized water.

Due to the photosensitivity of some chemicals (e.g., Amplex Red reagent), all experiments were performed in the dark. In all assays, neither deionized water (Milli-Q, Millipore Ibérica S.A., Madrid, Spain) nor appropriate dilutions of the vehicle used (DMSO) had significant pharmacological effects.

Data presentation and statistical analysis

Unless otherwise specified, results shown in the text and tables are expressed as mean ± standard error of the mean (S.E.M.) from *n* experiments. Significant differences between two means ($P < 0.05$ or $P < 0.01$) were determined by one-way analysis of variance (ANOVA) followed by the Dunnett's *post-hoc* test.

To study the possible effects of the test drugs (new compounds or reference inhibitors) on MAO isoform enzymatic activity, we evaluated the variation of fluorescence per unit of time (fluorescence arbitrary U/min) and indirectly the rate of hydrogen peroxide (H_2O_2) production, and therefore the pmol/min of resorufin produced in the reaction between H_2O_2 and Amplex Red reagent. For this purpose, several concentrations of resorufin were used to prepare a standard curve with X = pmol resorufin and Y = fluorescence arbitrary U. Note that the value of resorufin production is similar to the pmol of *p*-tyramine oxidized to *p*-hydroxyphenylacetaldehyde/min, since the stoichiometry of the reaction (*p*-tyramine oxidized by MAO isoforms/resorufin produced) is 1:1.

In these experiments, the inhibitory activity of the tested drugs (new compounds and reference inhibitors) is expressed as IC_{50}, i.e. the concentration of these compounds required for a 50% reduction of the control MAO isoform enzymatic activity, estimated by least-squares linear regression, using the program Origin 5.0 (Microcal Software, Inc., Northampton, MA, USA), with X = log of tested compound molar concentration and Y = the corresponding percentage of inhibition of control resorufin production obtained with each concentration. This regression was performed using data obtained with 4-6 different concentrations of each tested compound which inhibited the control MAO isoform enzymatic activity by between 20 and 80%. In addition we calculated the corresponding MAO-B selectivity indexes (Ratio = [IC_{50} (hMAO-A)]/[IC_{50} (hMAO-B)]).

Kinetic parameters (K_m and V_{max}) of hMAO-A and hMAO-B were estimated by least-squares linear regression, using the program Origin 5.0 (Microcal Software, Inc., Northampton, MA, USA), of the corresponding double-reciprocal Lineweaver-Burk plots with X = 1/*p*-tyramine molar concentration and Y = 1/reaction velocity (V). The Y-intercept and the slope of this regression have a values of $1/V_{max}$ and K_m/V_{max}, respectively.

Chromatographic conditions

Figure S1. Simultaneous HPLC diastereo- and enantioseparation of **3**.

Column, Chiralpak AS-H (250 mm x 4.6 mm I.D); eluent, n-hexane-2-propanol 90-10 (v/v); flow-rate: 1 ml min^{-1}; detector, UV and CD at 310 nm; temperature: 25 °C.

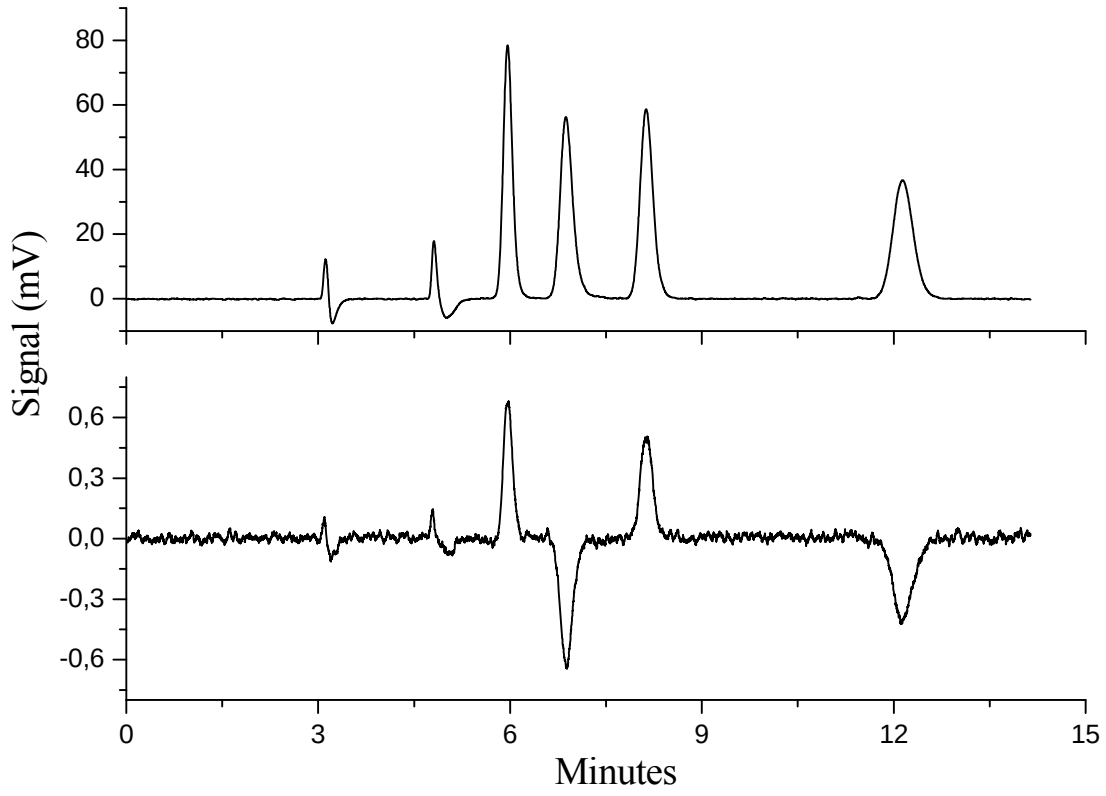

Figure S2. Simultaneous HPLC diastereo- and enantioseparation of **8**.

Column, Chiralpak AS-H (250 mm x 4.6 mm I.D); eluent, n-hexane-2-propanol 75-25 (v/v); flow-rate: 1 ml min^{-1}; detector, UV and CD at 280 nm; temperature: 25 °C.

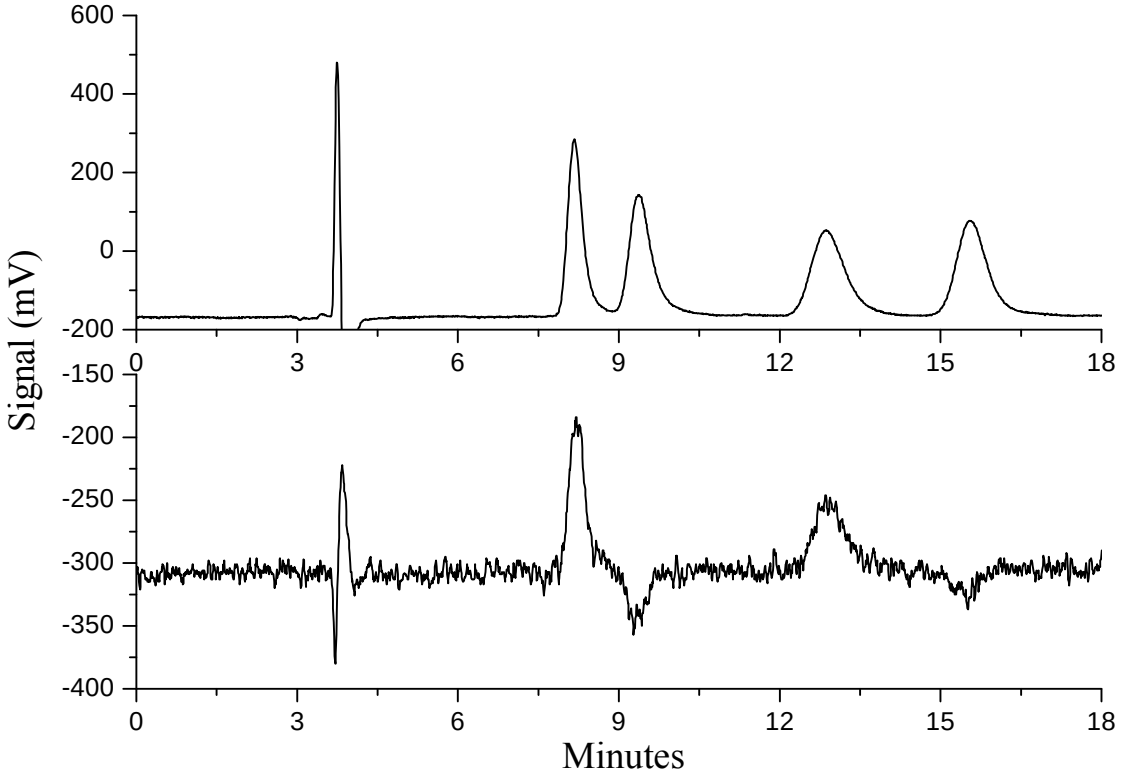

Figure S3. Simultaneous HPLC diastereo- and enantioseparation of **9**.

Column, Chiralpak AS-H (250 mm x 4.6 mm I.D); eluent, n-hexane-2-propanol 75-25 (v/v); flow-rate: 1 ml min^{-1}; detector, UV and CD at 280 nm; temperature: 25 °C.

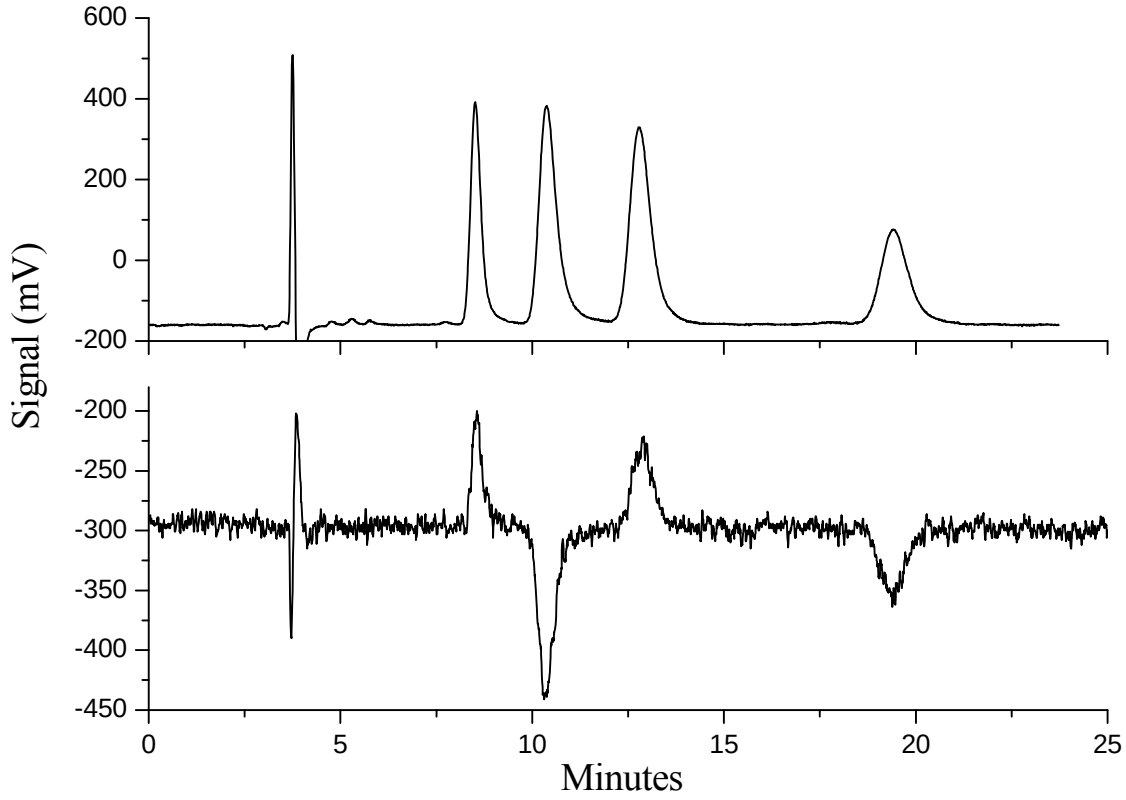

Molecular modelling studies

The molecular modelling of compound **5** was carried out following a similar approach reported in our previous communication.[1,2] For the presence in **5** of the asymmetric 3-methylcyclohexylidene moiety and the thiosemicarbazone imine N=C double bond, we have modeled the *E* and *Z* isomers separately and kept the *R* configuration fixed by Monte Carlo (MC) simulations and the molecular mechanics force field (MMFF). The conformational distribution in the energies window within 12.5 kcal/mol above the global minimum structure was larger for the (*R*)-E than for the (*R*)-*Z* stereoisomer, with 111 and 96 unique conformers, respectively. The MM energy evaluation of the global (*R*)-E and (*R*)-*Z* minimum conformers of **5** revealed differences in stability, which were lower than 0.03 and 0.27 kcal/mol when measured in different solvating environments. Both stereoisomers can exist in physiological conditions and can contribute almost equally to the binding properties within the hMAO isoforms. After converting the conformers of the *R* into the *S* enantiomer in both *E* and *Z* configurations, we used the four **5** ensembles to perform docking experiments on the hMAO pretreated enzyme models. In the rigid docking we included all the conformers obtained in the MC search. Then we fully energy-minimized the configurations of the eight possible combinations of hMAO isoforms and ligand stereoisomer. The thermodynamic interaction results are reported in Table S1.

Assuming that the enzyme inhibition is a function of the interaction energy, from a comparison with pIC_{50} a good correlation between theoretical and experimental data was observed. In all complexes the **5** *E* configuration was ranked as the most stable for recognition within the enzymes. In order to understand the thermodynamic results at the molecular level, we analyzed the four most stable complexes. In hMAO-A (Figure S4) **5** enantiomers showed a similar recognition pattern.

In both cases no hydrogen bonds were established between the ligand and the target. The methyl moiety on the asymmetric carbon of the six-membered ring and the thiazole represent the main (*R*)- and (*S*)-recognition difference allowing two additional hydrophobic contacts, to Met350 and Leu97, for the former enantiomer and one to Leu337 for the latter. In particular (*R*)-**5** was slightly closer to the FAD with respect to (*S*)-**5**. The main consequence of this was a better stacking interaction to Tyr407 and Tyr444. This justifies the slightly better recognition of this enantiomer compared to (*S*)-**5**, as demonstrated by the interaction energies in agreement with the experimental inhibition data.

In MAO-B (Figure S5) the molecular recognition of (*R*)-**5** and (*S*)-**5** was still quite similar. The aromatic and the thiazole moieties were located approximately in the same area, i.e., close to the FAD. (*R*)-**5** due to the different orientation of its 2-methylcyclohexylidene moiety was able to establish four adding hydrophobic contacts to Leu164, Leu167, Phe168 and Ile199. Moreover, such an enantiomer established an hydrogen bond to the Tyr326. The sum of these interactions, in particular the hydrogen bond, could explain the better hMAO-B recognition of (*R*)-**5** with respect to (*S*)-**5**.

All calculations were carried out with a Linux cluster of 16 Intel Xeon dual processors at 3.2 GHz with 2 Gb of RAM. Graphic manipulations and analysis of the docking experiments were performed with the Maestro Graphical User Interface, version 4.1.012, for Linux operating systems.[3] Ligplot, version 4.0,[4] and Pymol, version 0.98,[5] were used to create Figures S4 and S5. The first step was the conformational analysis of **5**. Five-thousand conformations were randomly generated and energy-minimized with the MMFF force field in GB/SA water and chloroform as implemented in the Macromodel package.[3] The conformational deduplication criterion was set as default, i.e., with a cutoff of 1 kcal/mol and an rms threshold of 0.25 Å. The mirror images of the (*S*)-*E* and (*S*)-*Z* stereoisomers were respectively obtained by inverting the sign of the *Z* atomic coordinates of the (*R*)-*E* and (*R*)-*Z* conformers of **5** obtained in the MC search using the MOLINE conversion module.[6] The second step of the modelling work was the pretreatment of the hMAO enzyme. The Protein Data Bank[7] crystallographic models of hMAO-A and hMAO-B, respectively known by the PDB codes 2BXR[8] and 1GOS,[9] were used for the docking experiments. Both structures were obtained as adducts with two similar compounds, clorgyline for 2BXR and pargyline for 1GOS, covalently linked to the FAD N5 nitrogen. After removal of the covalent bond between the FAD moiety and the cocrystallized inhibitor, pretreatment of the original PDB models consisted of a 48 kcal/mol constrained energy minimization of those residues out of a radius of 15 Å from N5 of the isoalloxazine ring in order to restore the natural planarity of the isoalloxazine FAD ring and relax the active site amino acids. The resulting energy minimum structure ligands were removed and used as receptor models. This was done with the AMBER* force field united atom notation and the GB/SA water model of solvation as implemented in MacroModel.[3] The third step was the docking into the hMAO receptor models. All energy minimum conformers of the four **5** stereoisomers were docked in the hMAO binding sites with the GLIDE docking method.[10]

Both pretreated enzyme models were submitted to map calculations using a box of about 110,000 Å^3 centered on the FAD N5 atom. The rigid docking of the 8 stereoisomers was done by generating a maximum number of 5000 configurations, scaling the ligand van der Waals radii by 10%. All complex configurations were fully energy-minimized with the AMBER* united atom and the GB/SA water model of solvation.[3] After full relaxation, the interaction energy of all complexes was computed according to the MOLINE method[6] and compared to the experimental inhibition data. In order to highlight the hMAO residues involved, the most stable fully energy-minimized configurations of four complexes were analyzed using the LigPlot program.[4]

References

1. Chimenti, F.; Maccioni, E.; Secci, D.; Bolasco, A.; Chimenti, P.; Granese, A.; Befani, O.; Turini, P.; Alcaro, S.; Ortuso, F.; Cardia, M. C.; Distinto, S. Selective inhibitory activity against MAO and molecular modeling studies of 2-thiazolylhydrazone derivatives. *J. Med. Chem.* **2007**, *50*, 707-712.
2. Chimenti, F.; Maccioni, E.; Secci, D.; Bolasco, A.; Chimenti, P.; Granese, A.; Carradori, S.; Alcaro, S.; Ortuso, F.; Yáñez, M.; Orallo, F.; Birilli, R.; Ferretti, R.; La Torre, F. Synthesis, stereochemical identification, and selective inhibitory activity against human monoamine oxidase-B of 2-methylcyclohexylidene-(4-arylthiazol-2-yl)hydrazones. *J. Med. Chem.* **2008**, *51*, 4874-4880.
3. *MacroModel*, version 7.2; Schroedinger Inc.: Portland, OR, 1998-2001.
4. Wallace, A. C.; Laskowski, R. A.; Thornton, J. LIGPLOT: a program to generate schematic diagrams of protein-ligand interactions. *Protein Eng*. **1995**, *8*, 127-134.
5. DeLano, W. L. The PyMOL Molecular Graphics System; DeLano Scientific: San Carlos, CA, 2002; http://www.pymol.org.
6. Alcaro, S.; Gasparrini, F.; Incani, O.; Caglioti, L.; Pierini, M.; Villani, C. A quasi flexible automatic docking processing for studying stereoselective recognition mechanisms. Part II. Prediction of ΔΔG of complexation and 1H-NMR NOE. J. Comput. Chem. **2007**, *28*, 1119-1128.
7. Berman, H. M.; Westbrook, J.; Feng, Z.; Gilliland, G.; Bhat, T. N.; Weissig, H.; Shindyalov, I. N.; Bourne, P. E. The Protein Data Bank. *Nucleic Acids Res*. **2000**, *28*, 235-242.
8. De Colibus, L.; Li, M.; Binda, C.; Lustig, A.; Edmondson, D. E.; Mattevi, A. Three-dimensional structure of human monoamine oxidase A (MAO A): relation to the structures of rat MAO A and human MAO B. *Proc. Natl. Acad. Sci. U.S.A.* **2005**, *36*, 12684-12689. (data deposition: www.pdb.org (PDB ID codes 2BXR, 2BXS, and 2BYB).
9. Binda, C.; Newton-Vinson, P.; Huba´lek, F.; Edmondson, D. E.; Mattevi, A. Structure of human monoamine oxidase B, a drug target for the treatment of neurological disorders. *Nat. Struct. Biol.* **2002**, *9*, 22–26. (data deposition: www.pdb.org (PDB ID code 1GOS).
10. Eldridge, M. D.; Murray, C. W.; Auton, T. R.; Paolini, G. V.; Mee, R. P. Empirical scoring functions: 1. The development of a fast empirical scoring function to estimate the binding affinity of ligands in receptor complexes. *J. Comput.-Aided Mol. Des.* **1997**, *11*, 425–445.

Table S1. Thermodynamic docking results of **5**·hMAO complexes and comparison with experimental inhibition data.

enzyme	C*	C=N	$\Delta\Delta E_{int}$ [a]	pIC_{50} [c]
hMAO-A	*R*	*E*	-9.20 [b]	4.41
		Z	[d]	
	S	*E*	-14.20 [b]	5.00
		Z	-13.50 [b]	
hMAO-B	*R*	*E*	-41.50 [b]	7.70
		Z	-38.13 [b]	
	S	*E*	-36.80 [b]	6.59
		Z	-36.14 [b]	

[a] In kcal/mol. [b] ΔΔ interaction energy minimum. [c] pIC_{50} = -log IC_{50}. [d] No docking solution, all configurations were rejected by energy.

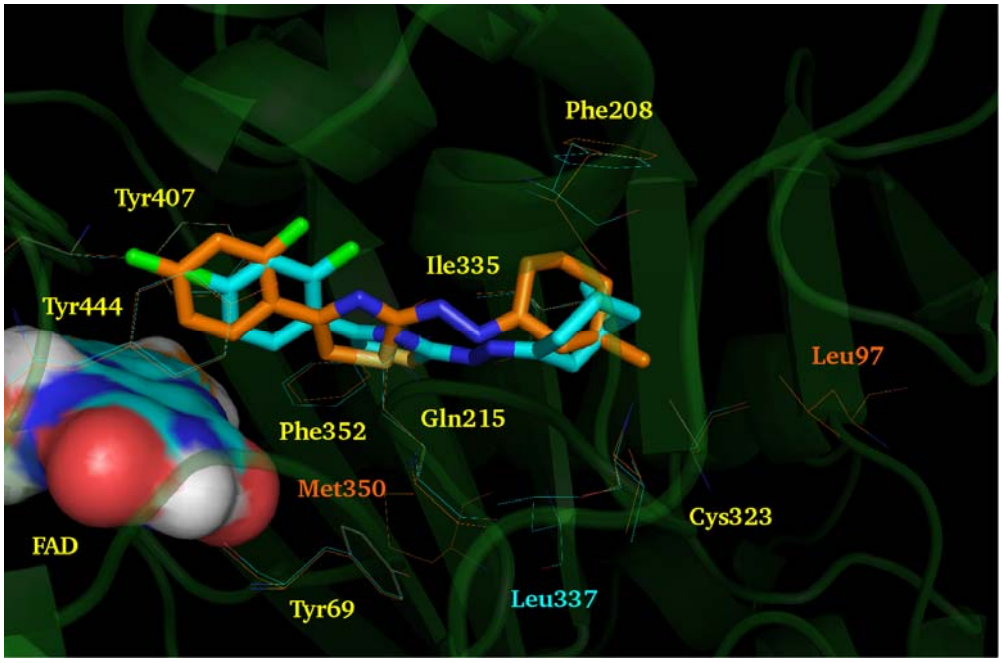

Figure S4: Superimposition of best fully energy minimized hMAO-A poses of (*R*)-**5** and (*S*)-**5** on protein Cα atoms. The ligand is depicted as orange carbon and light-blue carbon polytube models, respectively. The FAD cofactor is displayed with surface color coded carbons. The interacting residues with (*R*)-**5** and (*S*)-**5** are reported as orange and light-blue carbon wires, respectively. Hydrogen atoms are omitted for clarity.

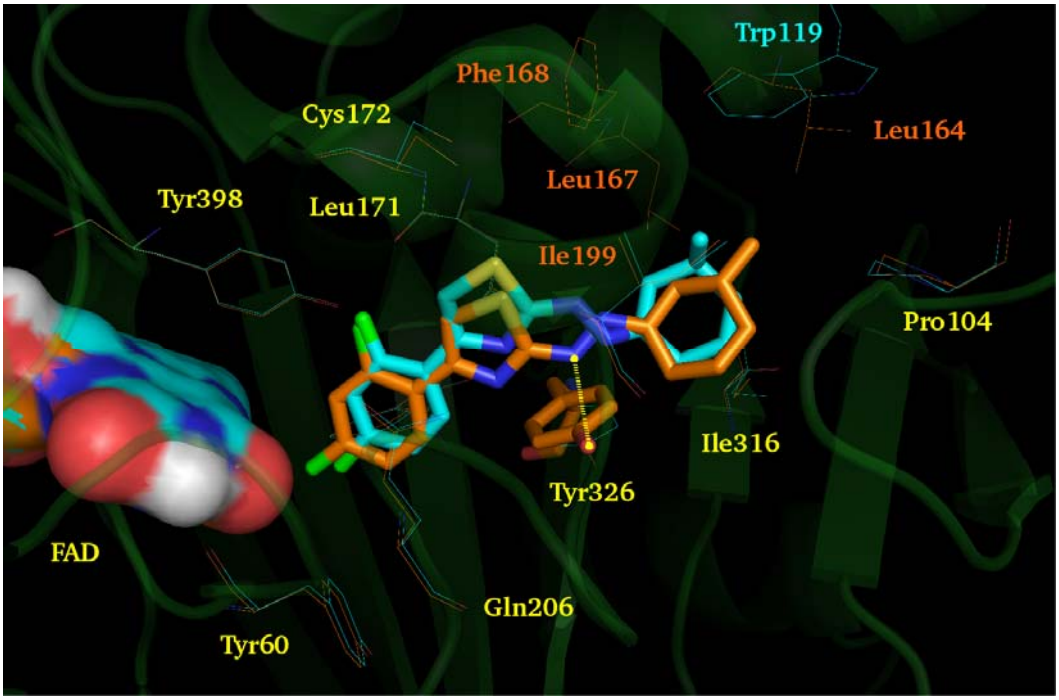

Figure S5: Superimposition of best fully energy minimized hMAO-B poses of (*R*)-**5** and (*S*)-**5** on protein Cα atoms. The ligand is depicted as orange carbon and light-blue carbon polytube models, respectively. The FAD cofactor is displayed with surface color coded carbons. The interacting residues with (*R*)-**5** and (*S*)-**5** are reported as orange and light-blue carbon wires, respectively. Hydrogen atoms are omitted for clarity. The hydrogen bond between the (*R*)-**5** and Tyr326 is reported as yellow dotted lines. Tyr326 establishing hydrogen bond with (*R*)-**5** is rendered as polytubes.

Elemental analysis and chemical data of new derivatives.

1-(4-phenylthiazol-2-yl)-2-(3-methylcyclohexylidene)hydrazine (1). 89% yield; mp 163-164 °C; ^{1}H NMR ($CDCl_3$) 1.01-1.03 (d, J = 6.3 Hz, 3H, CH_3), 1.19-1.22 (m, 1H, cyclohexyl), 1.80-1.85 (m, 3H, cyclohexyl), 1.99-2.03 (m, 3H, cyclohexyl), 2.50-2.53 (t, 1H, cyclohexyl), 2.99-3.05 (t, 1H, cyclohexyl), 6.68 (s, 1H, C_5H-thiazole), 7.45-7.51 (m, 3H, Ar), 7.71-7.73 (d, J_o = 7.8 Hz, 2H, Ar), 12.51 (s, 1H, NH, D_2O exch.).
(*R*)-1-(4-phenylthiazol-2-yl)-2-(3-methylcyclohexylidene)hydrazine (1a). 99% yield; mp 187-188 °C; ^{1}H NMR ($CDCl_3$) 0.88-0.89 (d, J = 6.2 Hz, 3H, CH_3), 1.18-1.20 (m, 1H, cyclohexyl), 1.60-2.06 (m, 6H, cyclohexyl), 2.53-2.59 (m, 1H, cyclohexyl), 2.97-3.00 (m, 1H, cyclohexyl), 6.56 (s, 1H, C_5H-thiazole), 7.11-7.15 (m, 2H, Ar), 7.57-7.59 (m, 3H, Ar), 12.41 (bs, 1H, NH, D_2O exch.).
(*R*)-1-(4-(4-fluorophenyl)thiazol-2-yl)-2-(3-methylcyclohexylidene)hydrazine (3a). 99% yield; mp 191-192 °C; ^{1}H NMR ($CDCl_3$) 0.99-1.01 (d, J = 6.3 Hz, 3H, CH_3), 1.28-1.29 (m, 1H, cyclohexyl), 1.68-1.99 (m, 6H, cyclohexyl), 2.50-2.51 (m, 1H, cyclohexyl), 2.99-3.01 (m, 1H, cyclohexyl), 6.60 (s, 1H, C_5H-thiazole), 7.16-7.18 (d, J_o = 7.8 Hz, 2H, Ar), 7.70-7.73 (d, J_o = 7.9 Hz, 2H, Ar), 12.79 (s, 1H, NH, D_2O exch.).
1-(4-(2,4-dichlorophenyl)thiazol-2-yl)-2-(3-methylcyclohexylidene)hydrazine (4). 90% yield; mp 175-176 °C; ^{1}H NMR ($CDCl_3$) 1.03-1.04 (d, J = 6.4 Hz, 3H, CH_3), 1.20-1.22 (m, 1H, cyclohexyl), 1.83-1.87 (m, 3H, cyclohexyl), 1.95-2.03 (m, 3H, cyclohexyl), 2.50-2.53 (t, 1H, cyclohexyl), 2.98-3.03 (t, 1H, cyclohexyl), 6.98 (s, 1H, C_5H-thiazole), 7.47 (s, 1H, Ar), 7.54 (s, 1H, Ar), 7.69 (s, 1H, Ar), 12.48 (s, 1H, NH, D_2O exch.).
(*R*)-1-(4-(2,4-dichlorophenyl)thiazol-2-yl)-2-(3-methylcyclohexylidene)hydrazine (4a). 95% yield; mp 169-170 °C; ^{1}H NMR ($CDCl_3$) 1.02-1.03 (d, J = 6.3 Hz, 3H, CH_3), 1.20-1.26 (m, 2H, cyclohexyl), 1.81- 2.24 (m, 5H, cyclohexyl), 2.48-2.53 (t, 1H, cyclohexyl), 2.97-3.03 (t, 1H, cyclohexyl), 6.96 (s, 1H, C_5H-thiazole), 7.42 (s, 1H, Ar), 7.54 (s, 1H, Ar), 7.63 (s, 1H, Ar), 12.88 (bs, 1H, NH, D_2O exch.).
1-(4-(2,4-difluorophenyl)thiazol-2-yl)-2-(3-methylcyclohexylidene)hydrazine (5). 93% yield; mp 171-172 °C; ^{1}H NMR ($CDCl_3$) 1.01-1.02 (d, J = 6.2 Hz, 3H, CH_3), 1.07 (s, 1H, cyclohexyl), 1.60-2.09 (m, 6H, cyclohexyl), 2.50-2.53 (t, 1H, cyclohexyl), 2.99-3.03 (t, 1H, cyclohexyl), 6.94 (s, 1H, C_5H-thiazole), 7.02 (s, 2H, Ar), 7.90 (s, 1H, Ar), 12.63 (s, 1H, NH, D_2O exch.).
(*R*)-1-(4-(2,4-difluorophenyl)thiazol-2-yl)-2-(3-methylcyclohexylidene)hydrazine (5a). 85% yield; mp 169-170 °C; ^{1}H NMR ($CDCl_3$) 1.01-1.03 (d, J = 6.4 Hz, 3H, CH_3), 1.17 (s, 1H, cyclohexyl), 1.60-2.19 (m, 6H, cyclohexyl), 2.49-2.53 (t, 1H, cyclohexyl), 2.98-3.02 (t, 1H, cyclohexyl), 6.94 (s, 1H, C_5H-thiazole), 7.03 (s, 2H, Ar), 7.83 (s, 1H, Ar), 12.73 (bs, 1H, NH, D_2O exch.).
(*R*)-1-(4-p-tolylthiazol-2-yl)-2-(3-methylcyclohexylidene)hydrazine (6a). 92% yield; mp 170-172 °C; ^{1}H NMR ($CDCl_3$) 1.06-1.07 (d, J = 6.3 Hz, 3H, CH3), 1.36 (s, 1H, cyclohexyl), 1.60-1.63 (m, 2H, cyclohexyl), 1.81 (s, 2H, cyclohexyl), 1.97-1.99 (m, 2H, cyclohexyl), 2.20-2.22 (m, 1H, cyclohexyl), 2.40 (s, 3H, 4'-CH_3Ar), 3.00-3.02 (m, 1H, cyclohexyl), 6.68 (s, 1H, C_5H-thiazole), 7.29 (s, 2H, Ar), 7.56 (s, 2H, Ar), 12.59 (s, 1H, NH, D_2O exch.).
1-(4-(4-nitrophenyl)thiazol-2-yl)-2-(3-methylcyclohexylidene)hydrazine (8). 93% yield; mp 167-168 °C; ^{1}H NMR ($CDCl_3$) 1.03-1.04 (d, J = 6.4 Hz, 3H, CH_3), 1.21-1.22 (m, 1H, cyclohexyl), 1.83-1.86 (m, 3H, cyclohexyl), 1.95-2.07 (m, 3H, cyclohexyl), 2.50-2.53 (t, 1H, cyclohexyl), 2.99-3.01 (t, 1H, cyclohexyl), 6.94 (s, 1H, C_5H-thiazole), 7.92-7.94 (d, J_o = 8.1 Hz, 2H, Ar), 8.35.8.37 (d, J_o = 8.2 Hz, 2H, Ar), 12.50 (s, 1H, NH, D_2O exch.).
(*R*)-1-(4-(4-nitrophenyl)thiazol-2-yl)-2-(3-methylcyclohexylidene)hydrazine (8a). 93% yield; mp 167-168 °C; ^{1}H NMR ($CDCl_3$) 1.01-1.05 (d, J = 6.5 Hz, 3H, CH_3), 1.19-1.20 (m, 1H, cyclohexyl), 1.83-1.98 (m, 5H, cyclohexyl), 2.05-2.07 (m, 1H, cyclohexyl), 2.50-2.52 (m, 1H, cyclohexyl), 2.69-2.72 (m, 1H, cyclohexyl), 7.05 (s, 1H, C_5H-thiazole), 7.92-7.94 (d, J_o = 8.0 Hz, 2H, Ar), 8.25.8.27 (d, J_o = 8.0 Hz, 2H, Ar), 12.48 (s, 1H, NH, D_2O exch.).
(*R*)-1-(4-(4-cyanophenyl)thiazol-2-yl)-2-(3-methylcyclohexylidene)hydrazine (9a). 99% yield; mp 187-188 °C; ^{1}H NMR ($CDCl_3$) 0.93-0.96 (d, J = 6.4 Hz, 3H, CH_3), 1.15 (s, 1H, cyclohexyl), 1.60-1.70 (m, 4H, cyclohexyl), 1.82-1.90 (m, 3H, cyclohexyl), 2.93 (s, 1H, cyclohexyl), 7.54 (s, 1H, C_5H-thiazole), 7.83-7.85 (d, J_o = 7.9 Hz, 2H, Ar), 8.00-8.02 (d, J_o = 7.9 Hz, 2H, Ar), 11.01 (bs, 1H, NH, D_2O exch.).

Compound	Elemental analysis			FW	CLogP	Formula
	C Calcd./Found	H Calcd./Found	N Calcd./Found			
1	67.33/67.30	6.71/6.70	14.72/14.71	285.41	4.86	$C_{16}H_{19}N_3S$
(*R*)-1	67.33/67.32	6.71/6.72	14.72/14.70	285.41	4.86	$C_{16}H_{19}N_3S$
(*R*)-3	63.34/63.35	5.98/5.98	13.85/13.87	303.40	5.01	$C_{16}H_{18}FN_3S$
4	54.24/54.22	4.84/4.85	11.86/11.85	354.30	6.04	$C_{16}H_{17}Cl_2N_3S$
(*R*)-4	54.24/54.26	4.84/4.83	11.86/11.87	354.30	6.04	$C_{16}H_{17}Cl_2N_3S$
5	59.79/59.80	5.33/5.33	13.07/13.06	321.39	5.15	$C_{16}H_{17}F_2N_3S$
(*R*)-5	59.79/59.81	5.33/5.34	13.07/13.08	321.39	5.15	$C_{16}H_{17}F_2N_3S$
(*R*)-6	68.19/68.21	7.07/7.08	14.03/14.02	299.43	5.36	$C_{17}H_{21}N_3S$
8	58.16/58.18	5.49/5.48	16.96/16.97	330.40	4.61	$C_{16}H_{18}N_4O_2S$
(*R*)-8	58.16/58.18	5.49/5.50	16.96/16.95	330.40	4.61	$C_{16}H_{18}N_4O_2S$
(*R*)-9	65.78/65.76	5.84/5.85	18.05/18.06	310.42	4.31	$C_{17}H_{18}N_4S$